

OPEN ACCESS

EDITED BY

Giandomenico Foti, Mediterranea University of Reggio Calabria,

REVIEWED BY Luigi Jovane, University of São Paulo, Brazil Hongyu Ye, Tsinghua University, China

*CORRESPONDENCE

Huiqiang Yao

⋈ hqyao@163.com

Xiguang Deng

dengxg68@163.com

Gaowen He

≥ hegaowen@163.com

[†]These authors have contributed equally to this work

RECEIVED 11 July 2025 ACCEPTED 23 September 2025 PUBLISHED 21 October 2025

CITATION

Wang H, Yi L, Wang F, Li Y, Cai Y, Zhang Z, Yu M, Deng X, Yang Y, Yao H, Deng X and He G (2025) Surficial sedimentary properties of Makran accretionary prism and its application to natural gas hydrate distribution. *Front. Mar. Sci.* 12:1664343. doi: 10.3389/fmars.2025.1664343

COPYRIGHT

© 2025 Wang, Yi, Wang, Li, Cai, Zhang, Yu, Deng, Yang, Yao, Deng and He. This is an open-access article distributed under the terms of the Creative Commons Attribution License (CC BY). The use, distribution or reproduction in other forums is permitted, provided the original author(s) and the copyright owner(s) are credited and that the original publication in this journal is cited, in accordance with accepted academic practice. No use, distribution or reproduction is permitted which does not comply with these terms.

Surficial sedimentary properties of Makran accretionary prism and its application to natural gas hydrate distribution

Haifeng Wang^{1,2†}, Liang Yi^{2†}, Fenlian Wang¹, Yibing Li², Yun Cai², Zhen Zhang¹, Miao Yu¹, Xianze Deng¹, Yong Yang¹, Huigiang Yao^{1*}, Xiguang Deng^{1*} and Gaowen He^{1*}

¹Ministry of Natural Resources (MNR) Key Laboratory of Marine Mineral Resources, Guangzhou Marine Geological Survey, Guangzhou, Guangdong, China, ²State Key Laboratory of Marine Geology, Tongji University, Shanghai, China

The Makran accretionary prism (MAP) resulted from the low-angle, slow-rate subduction of the Arabian Plate beneath the Eurasian Plate. The MAP is an active continental margin, with natural gas hydrate (NGH). In this study, we report an integrated study on surficial sediments, in terms of sediment grain-size, clay minerals and elements. The main results are as follows: (1) the surficial sediments were mainly controlled by hydrodynamic conditions of the Indus River. Along the Indus River channel, it is mainly infilled with silt, while clays are mainly distributed in the accretionary prism. The turbidity records gradually decrease from east to west, along the Indus River channel. (2) Illite and chlorite are the dominate clay minerals, indicating that the surficial sediments were mainly from weathering processes in the Himalaya by the Indus River transport. The very-low contents of kaolinite and smectite indicate the lack of sediments from the Deccan Traps and the in situ hydrothermal materials. (3) Elements analysis indicates that elements Al, Mg, K, Fe, and Ti were terrigeneous, mainly distributed in the northern MAP, while elements Ca and P were from biogenic sources, mainly distributed in the southern part of the study area. In addition, elements U and Mo distribute generally coupled with bottom simulating reflector (BSR), which can be used as proxies of NGH identification. Therefore, we proposed that the covariation between NGH distribution, BSR identification, and trace elements Mo and U holds the potentials in NGH investigation.

KEYWORDS

sedimentary progress, sediment provenance, clay minerals, natural gas hydrate (NGH), Makran accretionary prism

1 Introduction

The Makran Accretionary Prism (MAP) in the northeastern Arabian Sea resulted from a low-angle (typically< 3°) subduction of the Arabian plate beneath the Eurasian plate (Grando and McClay, 2007). The complex geological structure of this region involves a series of imbricate thrust fractures, including a near east-west thrust fold belt and a deep-sea plain and its inter-transition zone (Gong et al., 2018; Zhang et al., 2003).

The MAP is separated from regions of continental collision in the east by the left-lateral Ornach-Nal fault and in the west by the Minab Fault system. The Jaz Murian and the Hamun-i-Mashkel depressions located between the Makran coastline and the Baluchistan volcanoes are interpreted as forearc basins (Jacob and Quittmeyer, 1979). This large trench-arc distance makes the Makran the widest forearc complex in the world, with an accretionary prism of up to 300km in width (Smith, 2013). The age of the oceanic crust in the study area was considered in the Cretaceous "quiet" zone, because there is no identifiable sea-floor magnetic anomalies between the MAP and Murray Ridge (Whitmarsh, 1979). And heat flow data also suggest an age of between 70–120 Ma (Hutchison et al., 1981; Smith, 2013).

Seismic surveys along the MAP reveal that the sediment thickness at its deformation front is very high, up to 7km (Kopp et al., 2000), with frequent turbidity layers in the north. Before the early Miocene, the Himalayas was the dominant sediment source, and since the Murray Ridge system uplifted, the Indus River was isolated (Gaedicke et al., 2002; Rodriguez et al., 2014). Subsequently, sand and aeolian dusts from the Arabian Peninsula, with riverine materials from the northern arid regions turned to be the main sediment source of the MAP (Kukowski et al., 2001; Mouchot et al., 2010).

Previous studies suggests that the deposition process of the MAP is controlled by several factors: (1) The Indus River in the northeast carries a high flux of terrestrial debris, while the floods carry coarse-grained terrestrial debris as turbidity deposit (Bourget et al., 2011); (2) Winter winds generated by low-pressure cyclones in the Mediterranean region cross the Arabian continent carry a large amount of dust materials into the Arabian Sea (Prins et al., 1999; Clemens and Prell, 2003); (3) Marine organisms in the Arabian Sea and erosional materials from the seafloor also have some contribution (von Rad et al., 1999; Luckge et al., 2001; Fleitmann et al., 2007; Thamban et al., 2007).

Natural gas hydrate (NGH) is an efficient, clean energy with a broad distribution in the world, and is considered as an ideal alternative energy in the future (Milkov, 2000). Global NGH investigations indicated that an NGH system usually locates on the slopes of passive continental margins, often in large contourite deposits, or in an accretionary wedge on subduction margins (Wang et al., 2010). Among them, unique geological units, such as faults, folds, landslides, mud diapirs, and mud volcanoes, are commonly identified (Xie et al., 2013), suggesting the great potential of the MAP as one of the important NGH regions in the world.

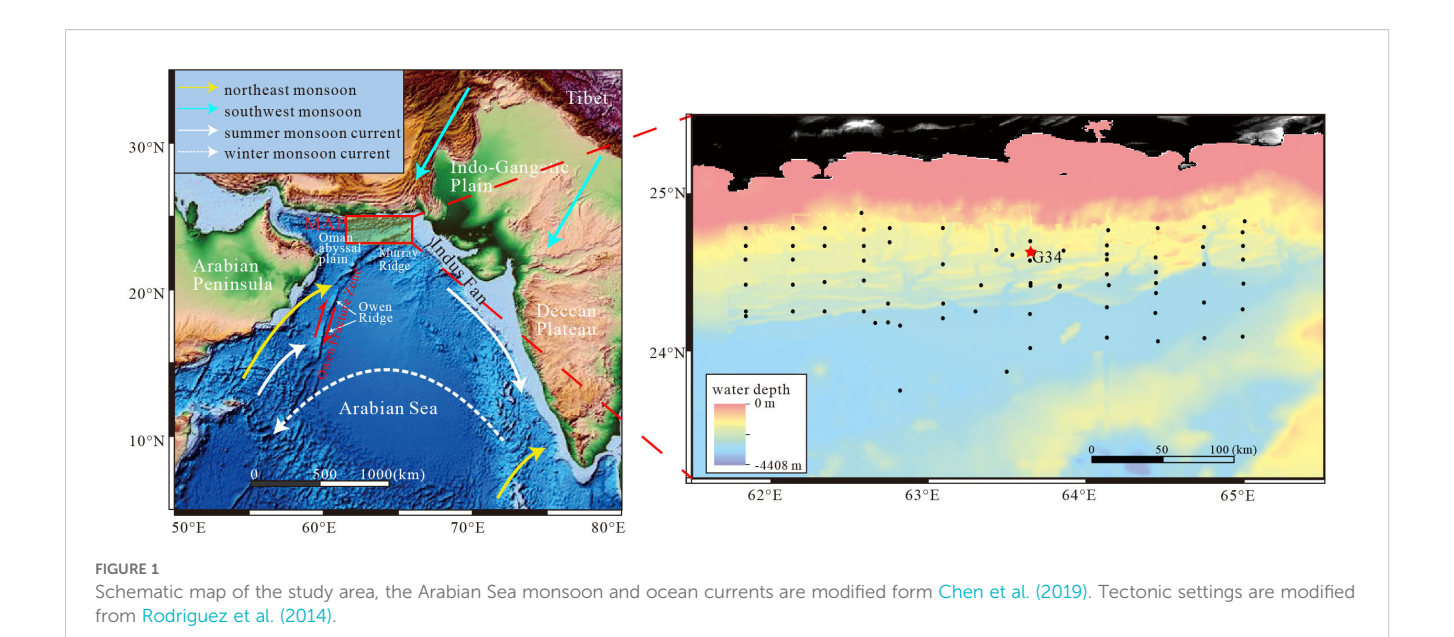
Several scientific survey, such as the joint expedition by the R/V Sonne in 1993 and 1997-1998, the R/V Meteor in 2007, and the R/V "Hai Yang Di Zhi Shi Hao" in 2019-2019, found many activities of fluid escape and NGH evidence in the MAP (von Rad et al., 2000; Kukowski et al., 2001; Bohrmann et al., 2008; Römer et al., 2012; Wei et al., 2021; Zhang et al., 2021), particularly the finding of NGH in water depths of 1000m and 2700m by the R/V Meteor in 2007 (Bohrmann et al., 2008). These studies included geological structures (mud diapirs, mud volcanoes, landslides and accretion wedges) (Su et al., 2014), geophysics (bottom simulating reflection, BSR) (Holbrook et al., 1996), mineralogy (carbonate rocks and authigenic minerals such as pyrite) (Zhang et al., 2011), marine halobios (bacterial mats, bivalves, mussels, and tube worms in the cold spring) (Campbell, 2006), and geochemical indicators (anions and cations in sediment pore water, hydrocarbon gases and sulfur isotopes) (Wu et al., 2010). Moreover, Grando and McClay (2007) proposed a "two-floor" model for NGH accumulation: the deep part is mainly controlled by thrust faults, while the shallow part is mainly controlled by normal faults. Smith et al. (2012) and Gong et al. (2016) reported that tectonic activity is the main controlling factor for NGH in the MAP. Zhang et al. (2021) suggested that mud diapir, mud volcanoes, gas chimney structures, and thrust faults are the main pathways for gas migration, playing an important role in controlling the accumulation and distribution of NGH in the MAP.

According to the NGH resource pyramid distribution, more than 90% of the global NGHs are reserved in submarine clayey silt or muddy sediments. Seabed sediments with different characteristics significantly impact the difficulty of natural gas hydrate exploitation. And in particular, clay minerals such as montmorillonite, illite, bentonite, and kaolinite play a significantly role in the storage and exploitation of NGH (Su et al., 2014; Ye et al., 2025). However, regional sedimentary pattern in the MAP and its relationship with NGH distribution are still unclear. To address the linkage between NGH and sedimentary properties, we report a study on surficial sediments collected by the China-Pakistan joint cruise by the R/V "Haiyang Dizhi Shi Hao" during 2018-2019, in terms of sediment grain size, geochemical properties, and clay minerals. Our results reveal the coupling relationship between sedimentary characteristics and NGH distribution.

2 Materials and methods

2.1 Studied samples

During 2018-2019, the R/V "Haiyang Dizhi Shi Hao" executed a systematic sampling of marine sediments in the MAP during the China-Pakistan Joint Cruise, by the Guangzhou Marine Geological Survey, China Geological Survey. A total of 80 sites of surficial sediments were obtained (Figure 1), with a gravity piston corer and a television grab. The collected sediments are mainly brown/grey mud and silt, and two sediment types are identified: fine-grained deposits with turbidite lamination (Shanmugam, 1994; 2002), and grey to brown clay, with biogenic debris and fossils.



2.2 Methods

Sediment cores are sampled at 20cm interval, and together with the surficial sediments, grain size, clay minerals and elemental contents are carried out in the Guangzhou Marine Geological Survey. Here, we exhibit all surface samples to illustrate sedimentary characteristics, and core sediments (core G34, 63.63659°E, 24.56111° N, 2046m water depth, with a length of 6.32m) were showed to interpret their vertical variabilities. This core was located at the center of our study area, directly above the NGH-rich zone. And also, the core is located in the transition zone between shallow-water and deepwater, receiving both terrigenous and marine sediments. As a result, it provides a comprehensive representation of the sedimentary characteristics of the study area. A total of 2580 sediment samples were collected for grain-size analysis, which were obtained from all sediment cores with an interval of ~20 cm. The samples were placed in an ultrasonic vibrator with ((NaPO₃)₆) for several minutes to facilitate dispersion, and measured using a Malvern Mastersizer 2000 grain size analyzer.

805 samples were collected for major and trace elements analysis, with an interval of ~60 cm. Major elements, including Si, Ti, Al, Fe, Mn, Mg, Ca, Na, K, and P, were analyzed using the X-ray Fluorescence Spectrometer (XRF; Nippon Science Primus II). The sample handling process for XRF analysis includes (1) placing the 200 mesh sample in a 105 °C oven to dry for 12h, (2) respectively placing 6.0g flux (Li₂B₄O₇: LiBO₂: LiF = 9:2:1) and 0.6g sample, 0.3g oxidant (NH₄NO₃)in a platinum crucible, being melted in a 1150 furnace for 14min. Finally, the crucible was removed and transferred to the refractory brick to cool, and the glass slide was removed for XRF analysis. Precision and accuracy were both better than 5%.

For trace elements contents analysis, the bulk sediments were completely dissolved by HF and HNO₃ solutions. About 50 mg sample was weighed and transferred into a pre-cleaned Teflon beaker followed by the addition of ultra-pure 1ml of HF and 1ml of HNO₃ solution. The beakers were then placed in steel cans and subjected to high

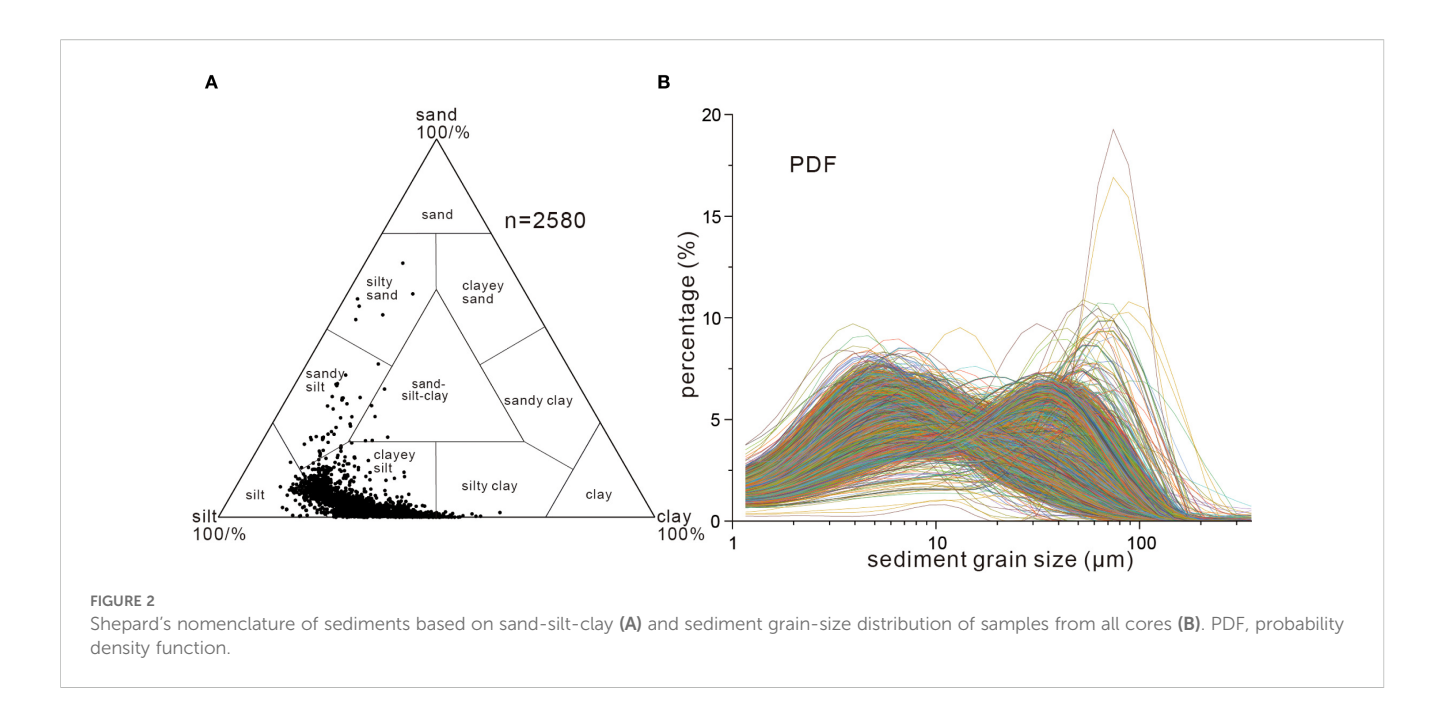
temperature (185 °C) and high pressure. After 36h, the solution was dried on a hotplate. The residues were fully digested using a mixture of concentrated 2ml $\rm HNO_3$ and 3ml Milli-Q water. Thereafter, the beakers were placed into steel cans at 120 °C for 5h. After cooling, the solution was diluted to 20ml with Milli-Q water. Trace elements were measured via ICP-MS (X Series2, Thermo Fisher Scientific, MA, USA). Precision and accuracy were both better than 5%.

442 clay minerals samples were collected, analyzed by X-ray diffraction (XRD) with an interval of 1m from the cores. The XRD clay mineral study was carried out on the<2 μ m fraction, which was separated by conventional Stokes' settling after the removal of carbonate and organic matter by acetic acid (15%) and hydrogen peroxide (10%), respectively. Clay minerals were then identified by XRD using a (Rigaku) D/Max 2500PC 18kW powder diffractometer (SYM125) in the Guangzhou Marine Geological Survey, with an X-ray wavelength λ =1.5418Å (CuK α), and a scanning rate of 2°(2 θ)/min at 0.02°(2 θ). Each sample was measured 3 times under conditions of air–drying, ethylene glycol solvation, and heating at 490 °C at atmospheric pressure. Clay minerals was identified according to the position of the (001) series of basal reflections observed on the XRD diagrams (Biscaye, 1965).

3 Results

3.1 Sediment grain sizes

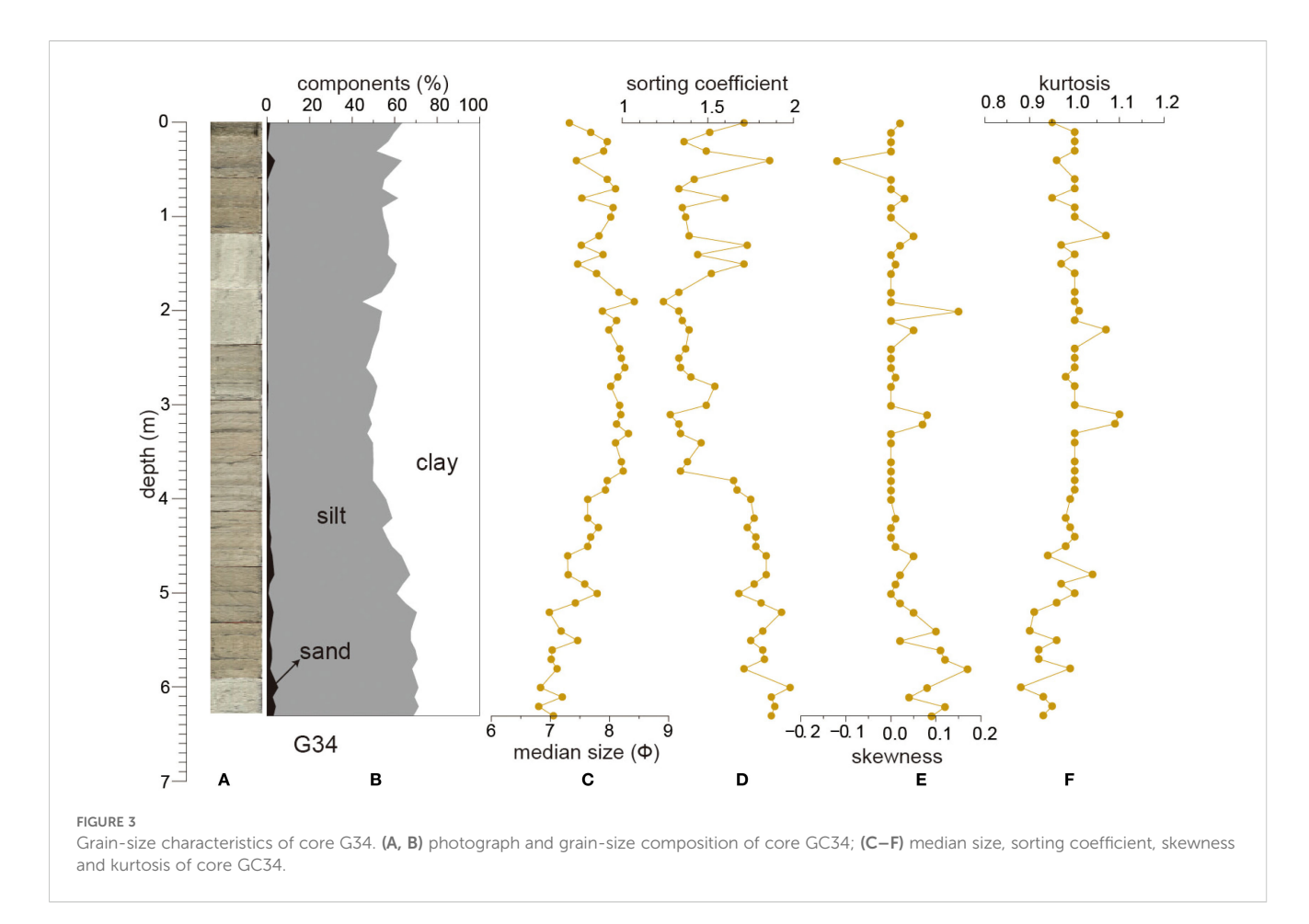
Silt is the dominant component in the sediments, with a range of 44.6% to 81.2%, followed by clay content of 16.8-53.4% and sand content up to 6.9%. In a Shepard's nomenclature (Shepard, 1954), most of the samples in the study area are clayey silt, with silty clay, silty sand, sandy silt, and very little silty sand and sand-silt-clay (Figure 2A). The grain-size distributions are bimodal, with modal sizes of 5-6 μm and 30-40 μm (Figure 2B), and only minor differences in the grain-size distributions between different sites, indicating a similar environment



in the MAP (Maynard et al., 1982). For core GC34 (Figure 3), the median size varies from $6.8 \, \Phi - 8.42 \, \Phi$, with an average value of $7.73 \, \Phi$. Sorting varies from 1.24 - 1.98, with an average value of 1.58. Skewness varies from -0.12 - 0.17, with an average value of 0.03. Kurtosis varies from 0.88 - 1.1, with an average value of 0.99. The median size of

sediment samples is generally stable with little variation. Silt (4-63 $\mu m)$ is the dominant component with an average value of 56.65%, while the clay (<4 μm) component is about ~40%, and the sand is only about 1%.

Ye et al. (2025) demonstrated that Global NGHs are more likely to occur in submarine silty and clay sediments. Taking the NGH sediment



samples in the Shenhu area of the South China Sea as an example, its distribution characteristics are between silt and clay. Our sediment samples are predominantly clayey silt, which is aligns with this pattern. A minority of coarse-grained samples were collected from water channels with strong hydrodynamic conditions in the study area.

For sediment cores, the sediment grain size gradually becomes finer from the east to the west (Figure 4), the sand content gradually decreases and the silt and clay fractions increase with the weakening of hydrodynamic conditions from the eastern Indian estuary towards the west; at the same time, several layers with coarser sediment grain size and higher sand fractions were found in the easternmost column samples G67, G61, G56 and G49, which may suggest the enhanced hydrodynamic of the estuary resulting in turbidity events (Burdanowitz et al., 2019).

For spatial distribution, regional sediments are fine, well sorted, positively skewed, and with moderate kurtosis, and become coarser to the south (Figure 4). In the southeast, the sediments become coarser, with a median size of about 5.0 Φ -6.8 Φ , bad sorted with the sorting coefficients (σ) up to 2.28, likely attributed to the influences of the Indus River.

3.2 Clay minerals

The sediments are dominated by illite and chlorite, with few kaolinite and smectite (Table 1). The illite content ranges from 40-60%, with an average value of 52.5%; chlorite content ranges from 26-52%, with an average value of 41.2%; kaolinite content ranges

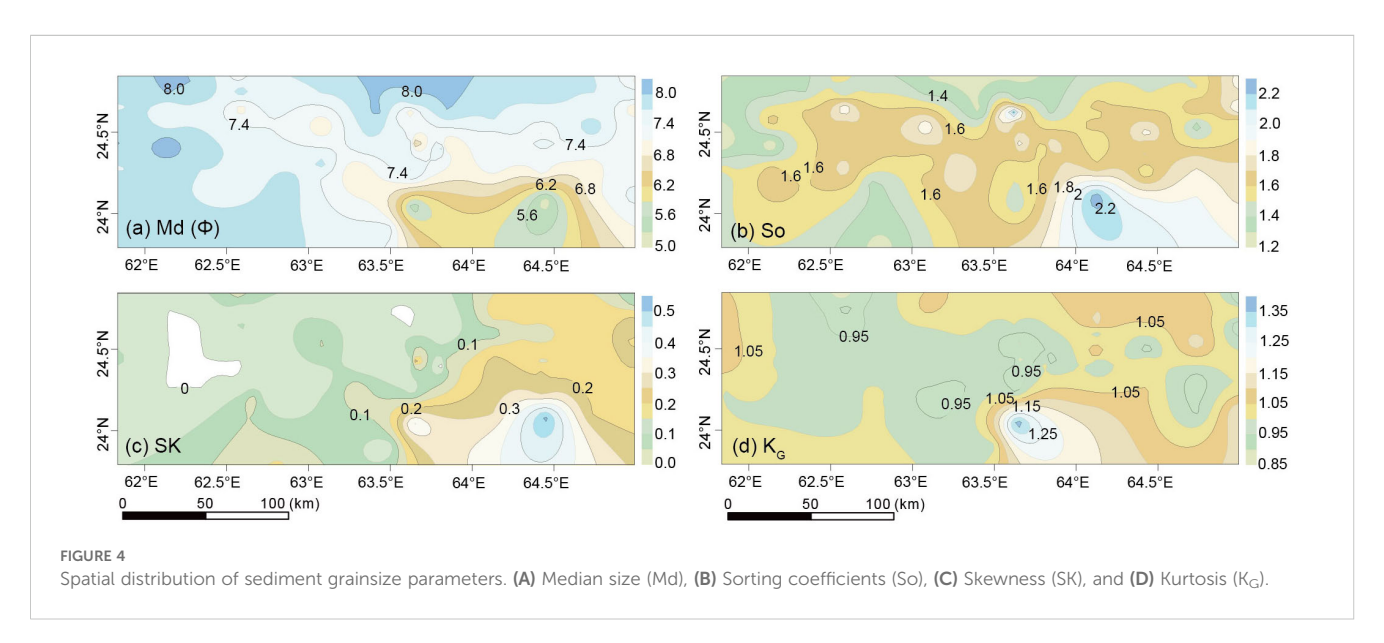


TABLE 1 Contents of clay minerals in the surface sediments and core G34 in the MAP.

Stations	Smectite	Illite	Kaolinite	Chlorite	Samples	Depth (m)	Illite	Chlorite	
G01	/	51 /		49	G34-1	0	48	52	
G02	/	52	/	48	G34-2	0.2	49	51	
G03	/	50	/	50	G34-3	0.4	49	51	
G04	/	52	/	48	G34-4	0.6	49	51	
G09	/	52	/	48	G34-5	0.8	52	48	
G11	/	52	/	48	G34-6	1	50	50	
G16	/	50	/	50	G34-7	1.2	51	49	
G19	/	53	/	47	G34-8	1.4	52	48	
G21	/	53	/	47	G34-9	1.6	51	49	
G23	/	49	/	51	G34-10	1.8	50	50	
G25	/	48	/	52	G34-11	2	51	49	
G27	/	50	/	50	G34-12	2.2	53	47	
G34	/	48	/	52	G34-13	2.4	52	48	
G35	1	48	/	52	G34-14	2.6	52	48	

(Continued)

TABLE 1 Continued

Stations	Smectite	Illite	Kaolinite	Chlorite	Samples	Depth (m)	Illite	Chlorite		
G40	/	49	/	/ 51 G3		2.8	52	48		
G43	/	48	/	52	G34-16	3	53	47		
G46	/	51.9	14.1	34.1	G34-17	3.2	52	48		
G47	/	55.3	15.8	29.0	G34-18	3.4	55	45		
G48	/	54.4	12.9	32.7	G34-19	3.6	53	47		
G49	/	53.6	13.3	33.1	G34-20	3.8	53	47		
G50	/	54.3	13.2	32.5	G34-21	4	55	45		
G51	/	51.6	14.2	34.3	G34-22	4.2	54	46		
G52	/	49.9	13.8	36.3	G34-23	4.4	51	49		
G53	1	47.4	16.7	35.9	G34-24	4.6	55	45		
G54	1.3	50.2	12.5	35.9	G34-25	4.8	54	46		
G55	0.8	51.9	13.9	33.4	G34-26	5	56	44		
G56	1	50.1	14.2	35.7	G34-27	5.2	56	44		
G57	1	47.6	15.0	37.4	G34-28	5.4	55	45		
G58	/	46.4	13.5	40.1	G34-29	5.6	53	47		
G59	/	50.0	11.6	38.5	G34-30	5.8	55	45		
G60	1	49.9	13.7	36.4	G34-31	6	57	43		
G61	1	51.7	15.4	32.8	G34-32	6.2	56	44		
G62	1	54.6	13.4	32.0						
G63	/	52.5	9.7	37.9						
G64	/	50.1	14.4	35.5						
G65	1	53.3	12.1	34.6						
G66	1	53.3	12.9	33.8						
G67	1	50.4	10.0	39.6						
G68	/	52.6	14.8	32.6						
G69	1	54.3	12.0	33.7						
G70	1	53.8	11.2	35.0						
G76	1	52	/	48						
G77	1	52	/	48						
G80	/	55	/	45						

[&]quot;/" indicates not detected.

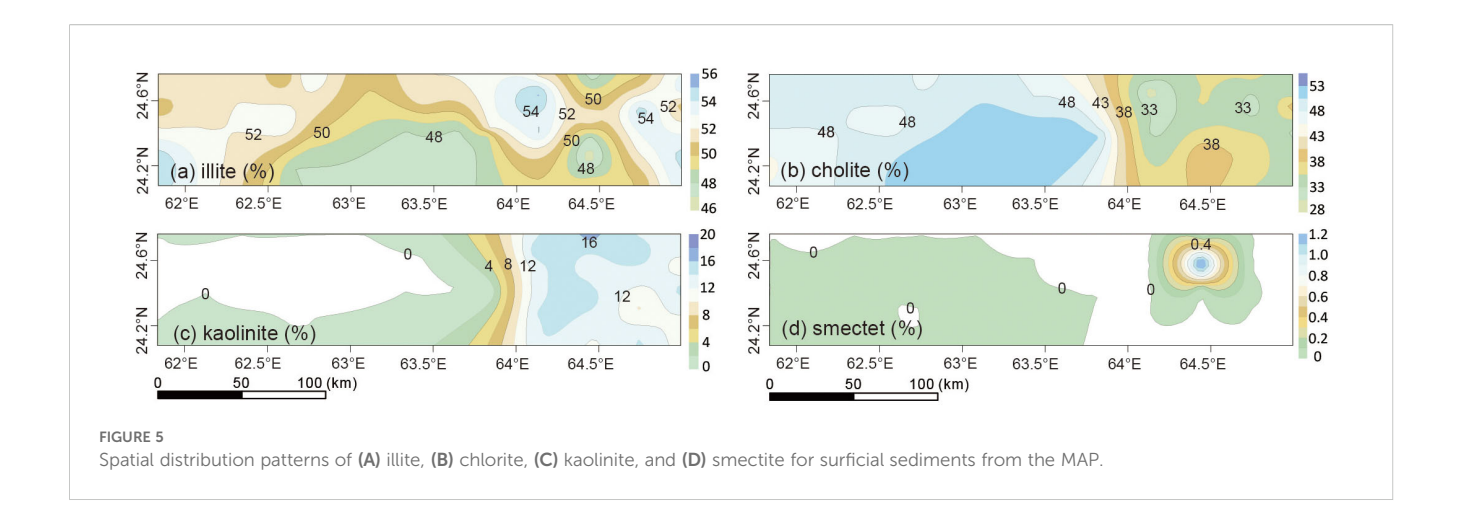
from none to 19.5%, with an average value of 6%; and smectite was the lowest mineral, ranging from 0-3% with an average value of 0.2%. The components of kaolinite and smectite are extremely low in the western part, generally below the detection limit. For core G34, smectite and kaolinite were not detected. Illite is the dominant clay mineral in the sediments, ranging between 48-57% and gradually decreasing from bottom to top. Changes in chlorite is opposite to that of illite.

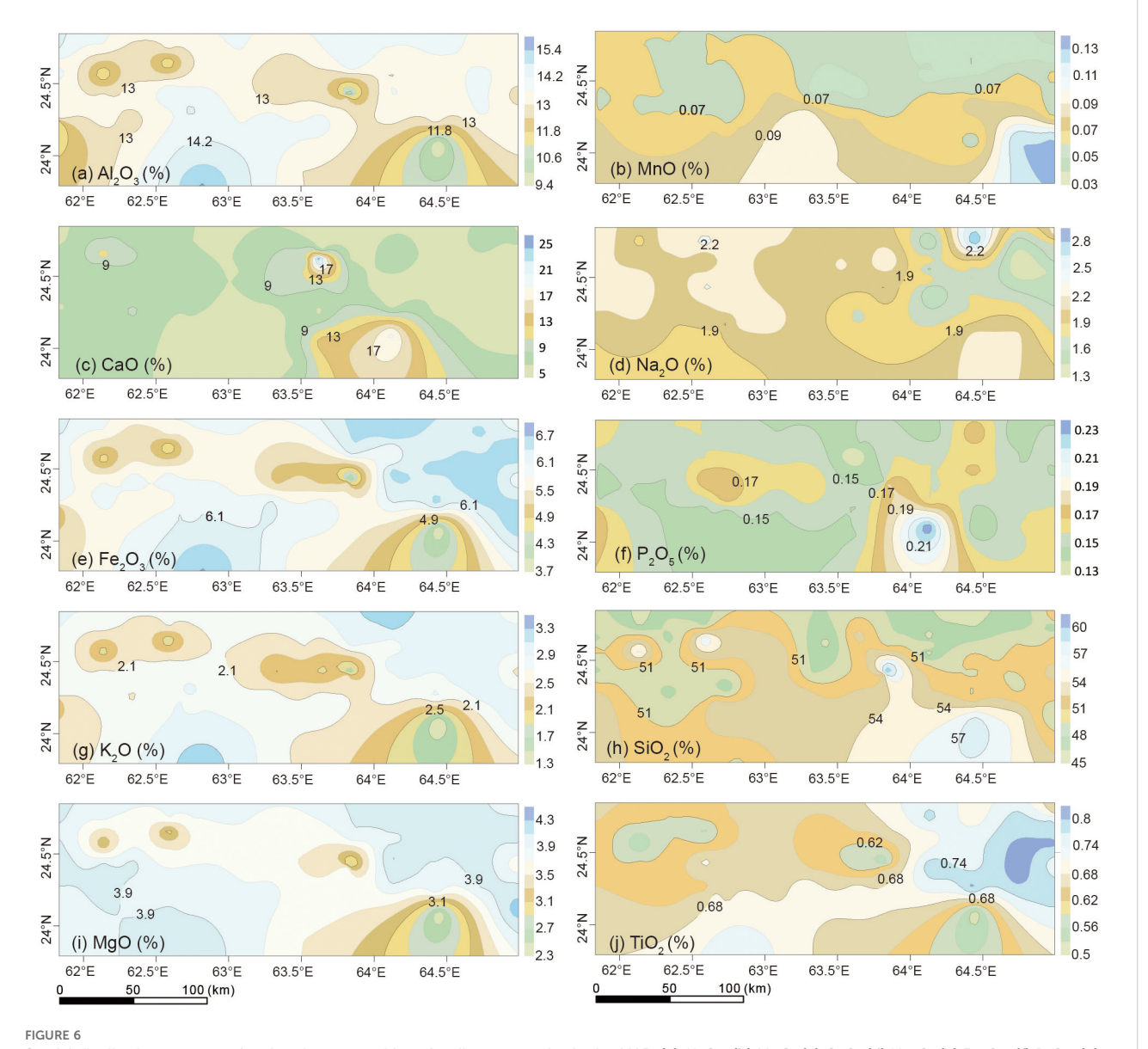
For spatial distribution (Figure 5), clay minerals are dominated by illite (46.4%-55.3%) and chlorite (29.0%-55.0%). Kaolinite increases in

the east, up to 16.7%, but decreases in the west. Smectite is rare in the whole area, usually less than 1%.

3.3 Oxides of major elements

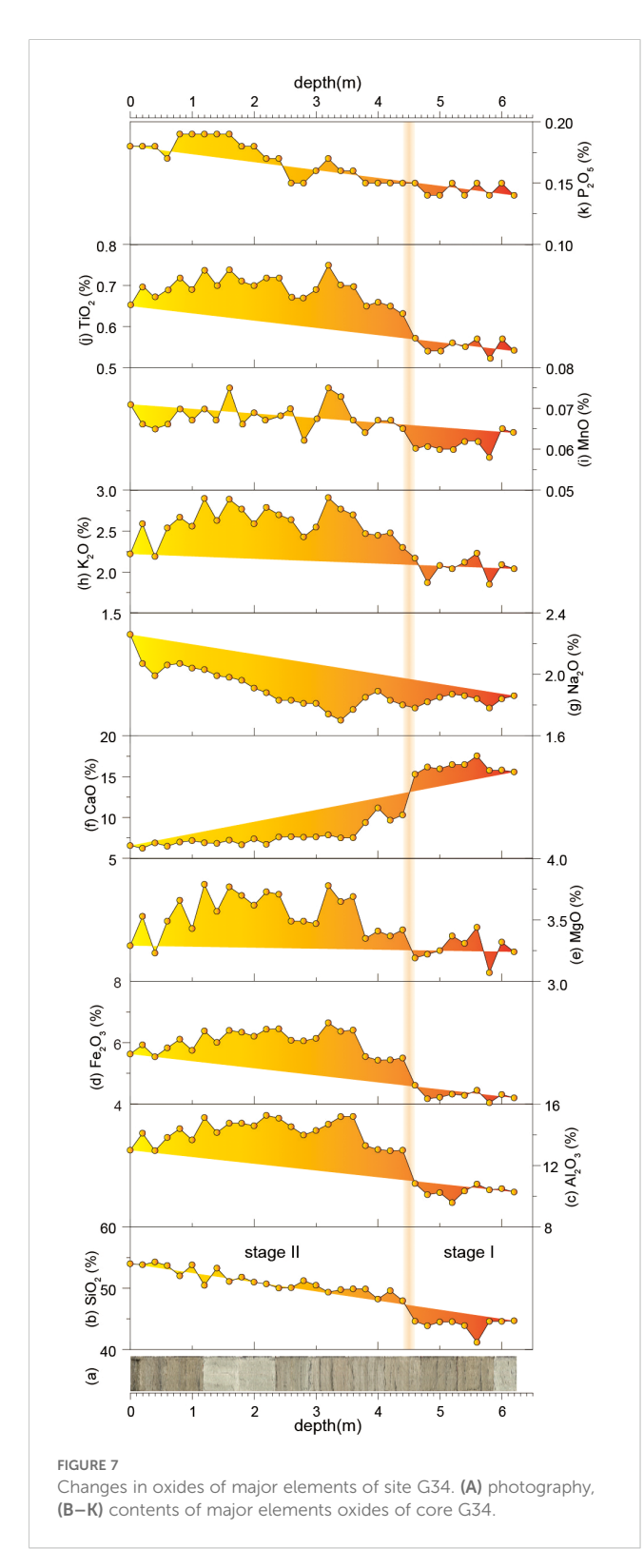
The results show that SiO_2 is the dominate composition in the sediments, generally over 50%. From the north to the south (Figure 6), SiO_2 increases from 46% to >55%. Al_2O_3 is the secondary major component, about 10% in the study area. For core G34, CaO shows an





Spatial distribution patterns of major elements oxides of sediment samples in the MAP. (a) Al_2O_3 , (b) MnO, (c) CaO, (d) Na_2O , (e) Fe_2O_3 , (f) P_2O_5 , (g) K_2O_5 , (h) SiO_2 , (i) MgO_5 , (j) TiO_2 .

opposite trend to other elements (Figure 7). Based on changes in CaO, two units were identified: in Stage I: below 4.6m, CaO is more than 15%, while within Stage II: above 4.6m, CaO is less than ~10%, likely indicating a decrease in marine biogenic components and an increase in terrigenous debris.



3.4 Trace elements

Spatial changes in trace elements are relatively stable than major elements (Figure 8). In specific, most of the trace elements, such as Cr, Cu, Mo, Ni, U, V, Zn, Zr, Rb, and REEs, are relatively similar, while element Sr ranges from 163 μ g/g (G50) to 1287 μ g/g (G52), consistent with that of Ca. In addition, Co, Cu, Ba, Cr, Rb, Ni and Zn contents in the sediments in the west are relatively high, while Sr concentrates in the east. For core G34, changes in trace elements can be similarly divided into two groups (Figure 9): in the stage I, Sr content is >1000 μ g/g and decreased sharply in the stage II (above 4.6m). Some trace elements, including Cr, Cu, Ni, V, Zn, and Rb, exhibit an opposite variation, while the others, such as Ba, Mo, U, Zr, and REEs, varies without any patterns.

3.5 Elemental correlations

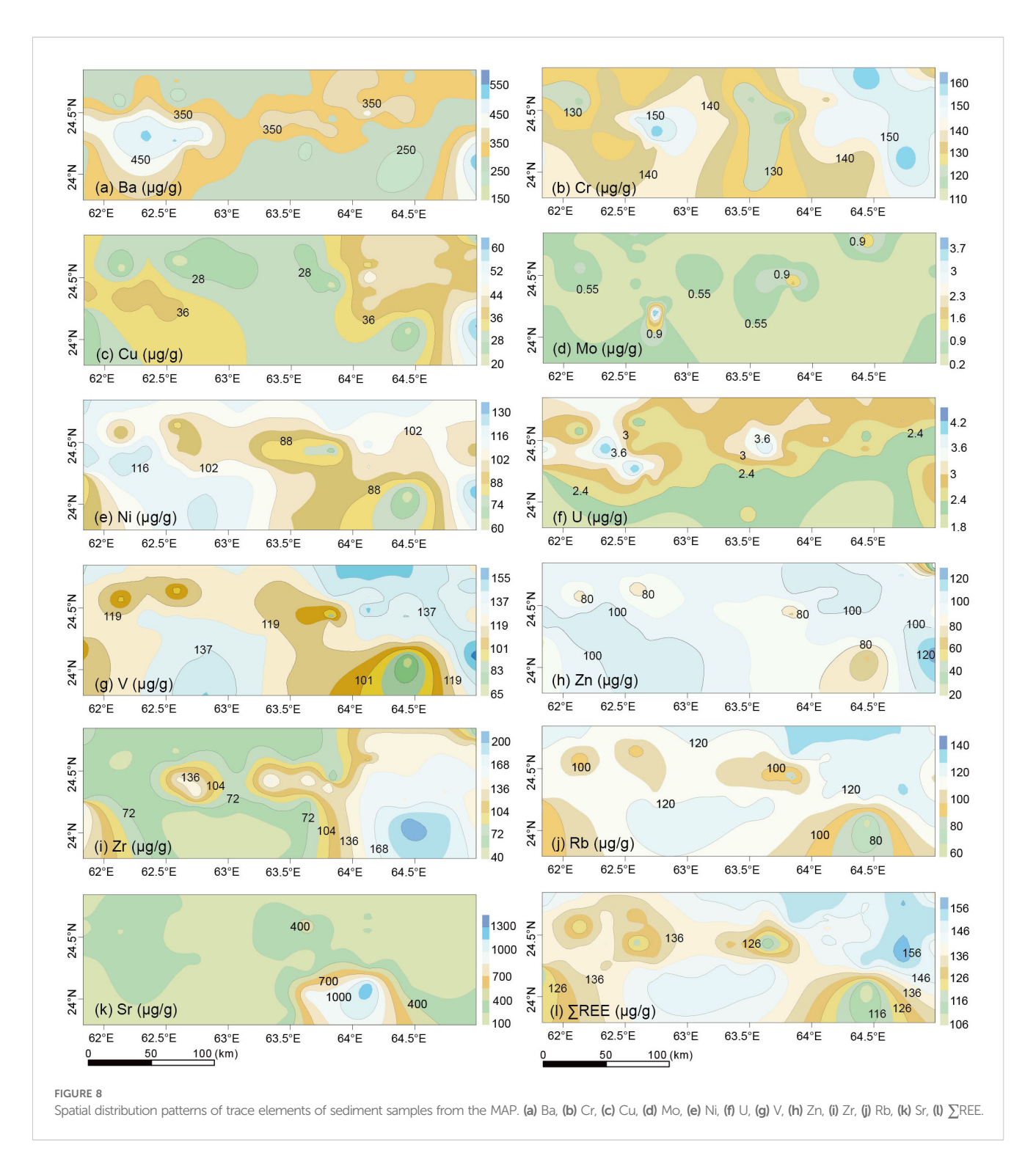
Correlation analyses on the elements in the surficial sediments of the study area were carried out and the results are shown in Table 2. As shown, Al₂O₃ is positively correlated with MgO, K₂O, TiO₂, Fe₂O₃, Co, Cr, Ni, Rb, Ga, V, and REE (Dubinin, 2004), and negatively correlated with CaO and Sr. Al₂O₃, MgO, K₂O and Fe₂O₃ are the main components from rock weathering, and TiO₂, Ga, and other elements are mainly derived from terrestrial detritus, which are mainly enriched in fine-grained sediments and endowed in a sorbed state in clay minerals. Hence, Al₂O₃, MgO, K₂O, Fe₂O₃ and TiO₂ likely represent terrestrial clastic fractions, and CaO and Sr are mainly related with biogenic carbonate fractions, which were less deposited in the MAP and mutually exclusive with other elements (Avinash et al., 2016).

Si in marine sediments consists of terrestrial debris and siliceous bioclastic. The terrigenous clastic source is usually dominated by silicate minerals, such as feldspar, quartz and clay minerals, and the biogenic phase is dominated by siliceous organisms, such as diatoms, sponges and radiolarians. Elemental correlation analysis of the surficial sediments shows that no agreement between SiO_2 and typical terrestrial components, such as Al_2O_3 , Fe_2O_3 , and Ga, was observed, suggesting that Si are mainly from biogenic materials. In addition, a good positive correlation between CaO and Sr was evident, inferring that these two elements are mainly derived from biogenic carbonate fractions.

4 Discussion

4.1 Sediment provenances

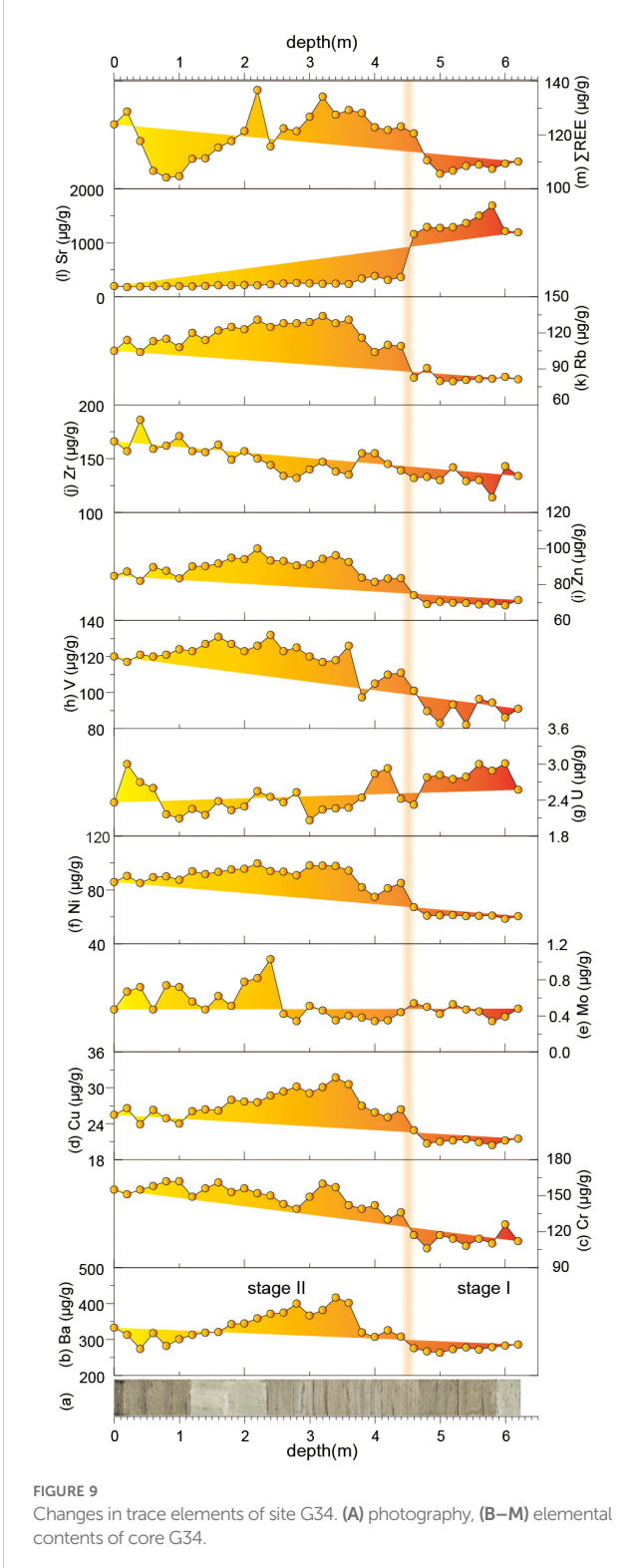
Clay minerals in the sediments of the East Arabian Sea are close to weathering and denudation materials from the Himalayas transported by the Indus River (Kolla et al, 1981; Alizai et al., 2012), from the Deccan Plateau transported by the Dabti and Narmada Rivers, and from the southern India (Kessarkar et al., 2003). The Indus River, the world's largest river, has about 250 \times 106t suspended materials to the Arabian Sea for each year. In the



Indus River catchment, Pre-Himalayan Cambrian metamorphic rocks and weathering denudation products from the Himalayas are characterized by crystallinity-rich illite and chlorite (Alizai et al., 2012). The southward coastal currents during the summer facilitate the southward transport of Indus suspensions, with an influence on the distribution of clay minerals in the East Arabian Sea from north to south (Thamban et al., 2002; Govil and Naidu, 2008; Yu et al., 2019). Comparing clay minerals in various sediments (Figure 10), it is inferred that: the surficial sediments in the MAP are mainly from

the Himalayan weathering denudation products imported by the Indus River, while the absence of montmorillonite and kaolinite indicates the MAP deposition less influenced by sedimentary denudation from the Deccan Plateau in the south.

The association between ratios SiO_2/Al_2O_3 and K_2O/Na_2O (Gong et al., 2021) suggests that all surficial and core sediments are deposited from an active continental margin (Figure 11A), agreeing well with the tectonic settings of the MAP. The association between Al_2O_3 , $CaO+Na_2O$, and K_2O , known as an



index of chemical weathering, namely Chemical Index of Alteration

(CIA) (Nesbitt and Young, 1982) as Equation 1:

$$CIA = Al_2O_3/(Al_2O_3 + K_2O + CaO + Na_2O) \times 100;$$
 (1)

Which indicates that the sediments in the research area are primarily the products of the initial weathering stage (Young and

Nesbitt, 1999; Liu et al., 2012). In addition, these sediments also distribute close to the trend line of granodiorite (Figure 11B), indicating that the parent rocks of these sediments are granodiorite (Xu and Shao, 2018).

Furthermore, inactive trace elements, such as V, Zn, Cr, Ni, and Zr, are primarily controlled by the nature of parent rocks in provenance, and play a crucial role in determining the nature of sediment sources. As shown in Figure 12, the concentrations of these elements in our research area are quite different from those in the surface sediments of the continental shelf off the Indus Delt (Khan et al., 2020), Arabian Sea (Schnetger et al., 2000; Sirocko et al., 2000), average Indus River sediments (Clift et al., 2010) and west coast Indian (Alagarsamy and Zhang, 2010). This discrepancy may suggest that the terrigenous clastic sediments are not the sole provenance in the study area.

Gong et al. (2021) analyzed the trace element compositions of two sediment cores from the MAP, and concluded that the surface sediments possibly contain the Makran-Bela Ophiolite from the northwestern part and Murray Ridge igneous rocks from the southeastern part. The Makran-Bela Ophiolite and Murray Ridge igneous rocks are characterized by an occurrence of basalt and basic ultramafic rocks (Khan and Liu, 2019; Burgath et al., 2002; Ghose et al., 2014). Meanwhile, ultramafic rocks tend to have a high content of Cr, Co, and Ni and basalts tend to have a high content of Cu (Zahid et al., 2015). These trace elements were transported in to the sediments, resulting in elevated concentrations.

Overall, the eastern part of the MAP receives weathering products from the Himalayas carried by the Indus River and wind dust from the Arabian Peninsula, likely with a small amount of volcanic and hydrothermal material from the ocean floors.

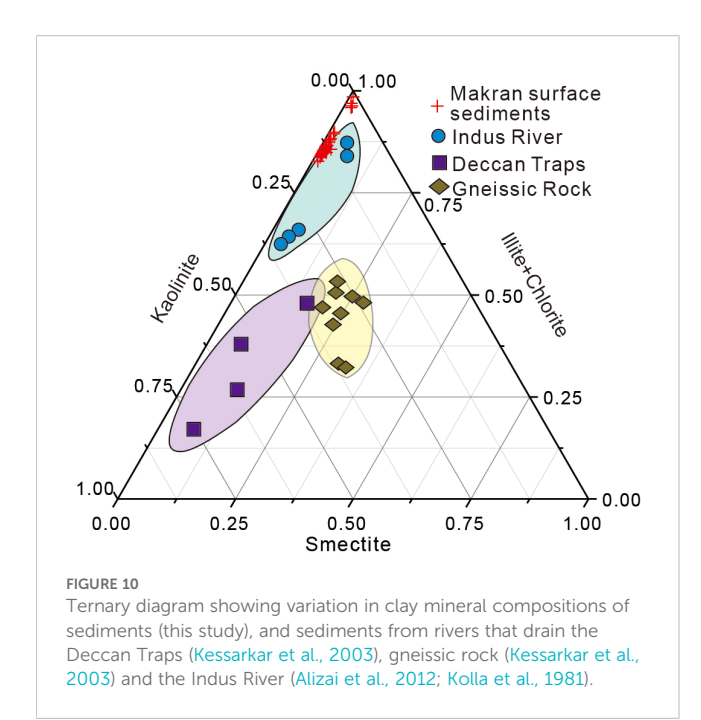
4.2 Relationship between NGH and surficial sediments

NGH are solid substances consisting of methane, ethane, carbon dioxide and other gases and water molecules under high pressure and low temperature (Zhang et al., 2003; Gong et al., 2016, 2018). Classic NGH exploration relies on geophysical methods, typically identifying the bottom simulating reflector (BSR) (Smith et al., 2014). Based on the BSR identification in the MAP (Smith et al., 2014), the sediment samples were classified into three categories: sediment samples over the BSR, and outside the BSR distribution (Figure 13A), respectively, and accordingly, a comparison between trace elements Mo and U similarly exhibits distinct relationships (Figures 13B-D), inferring the coupling between NGH distribution, BSR identification, and trace elements Mo and U. The contents of U and Mo in the sediment samples outside the BSR are generally less than 3 µg/g (Figure 13B), whereas the contents are significantly higher in the sediment samples over the BSR (Figure 13C).

The concentration relationships of redox-sensitive elements such as U and Mo can be used to interpret the marine depositional environment (Figure 14) (Guo et al., 2007; Algeo and

TABLE 2 Earth elements correlation coefficients of surficial sediments from Makran Accretionary Prism.

	SiO ₂	Al ₂ O ₃	CaO	MgO	K ₂ O	Na ₂ O	TiO ₂	P ₂ O ₅	MnO	Fe ₂ O ₃	Со	Cu	Pb	Ва	Cr	Ni	Zn	Rb	Ga	Sr	V	Zr
Al ₂ O ₃	0.18																					
CaO	-0.71	-0.78																				
MgO	0.02	0.93	-0.69																			
K ₂ O	0.00	0.95	-0.68	0.97																		
Na ₂ O	0.16	0.12	-0.15	0.01	-0.06																	
TiO ₂	0.25	0.81	-0.78	0.83	0.88	-0.30																
P_2O_5	-0.19	-0.24	0.13	-0.11	-0.16	0.07	-0.12															
MnO	0.42	0.19	-0.36	0.09	-0.06	0.18	0.16	0.07														
Fe ₂ O ₃	0.07	0.92	-0.72	0.94	0.97	-0.13	0.92	-0.09	0.16													
Со	0.03	0.74	-0.61	0.72	0.83	-0.07	0.75	-0.04	0.23	0.85												
Cu	-0.25	0.55	-0.32	0.73	0.73	-0.27	0.69	-0.05	0.00	0.74	0.83											
Pb	0.08	0.58	-0.54	0.69	0.72	-0.45	0.86	-0.03	0.13	0.80	0.78	0.80										
Ва	-0.09	0.44	-0.29	0.62	0.52	0.09	0.33	-0.09	0.02	0.48	0.75	0.65	0.48									
Cr	0.33	0.70	-0.79	0.72	0.75	-0.09	0.88	0.02	0.17	0.80	0.72	0.64	0.74	0.40								
Ni	-0.05	0.89	-0.56	0.91	0.87	0.25	0.59	-0.21	0.15	0.80	0.81	0.63	0.47	0.40	0.54							
Zn	-0.08	0.68	-0.44	0.74	0.74	-0.01	0.59	-0.14	0.12	0.70	0.73	0.71	0.58	0.70	0.55	0.75						
Rb	0.01	0.95	-0.67	0.95	0.97	0.03	0.83	-0.18	0.09	0.94	0.73	0.68	0.65	0.60	0.71	0.88	0.72					
Ga	0.11	0.98	-0.72	0.93	0.96	0.05	0.81	-0.24	0.17	0.93	0.76	0.59	0.61	0.50	0.68	0.89	0.69	0.95				
Sr	-0.48	-0.77	0.78	-0.65	-0.67	-0.09	-0.71	0.48	-0.17	-0.64	-0.48	-0.40	-0.45	-0.20	-0.61	-0.57	-0.46	-0.70	-0.71			
V	-0.03	0.91	-0.65	0.95	0.98	-0.04	0.85	-0.13	0.10	0.96	0.86	0.79	-0.45	0.60	-0.61	0.88	0.76	0.96	0.93	-0.65		
Zr	-0.07	0.07	-0.18	0.21	0.25	-0.46	0.52	0.28	-0.06	0.36	0.38	0.56	0.61	0.10	0.59	-0.07	0.17	0.18	0.05	-0.10	0.27	
REE	0.26	0.89	-0.79	0.87	0.91	-0.10	0.92	-0.20	0.14	0.91	0.73	0.58	0.75	0.40	0.77	0.71	0.63	0.91	0.89	-0.74	0.88	0.25



Rowe, 2012; Deng et al., 2017). U is a typical oxygen-loving element, which is reduced to tetravalent in an oxidizing environment and is enriched in sediments as a non-soluble state (Calvert and Pedersen, 1993; Tribovillard et al., 2006). Molybdenum is extremely sensitive to the oxidation-reduction environment of its environment; Mo^{6+} is the most common oxidation valence state and migrates in solution as $MoO_4^{\ 2-}$; under reducing conditions, molybdenum is attached to solid-phase sediments as Mo^{4+} or Mo^{5+} (Tribovillard et al., 2006). The U in seafloor cold spring sediments, Mo enrichment can occur. This is mainly because of the presence of large amounts of H_2S in the pore water because of the organoclastic sulfate reduction (OSR,

Equation 2), and Anaerobic Oxidation of Methane (AOM, Equation 3) reaction (März et al., 2008; Li et al., 2021), as follows:

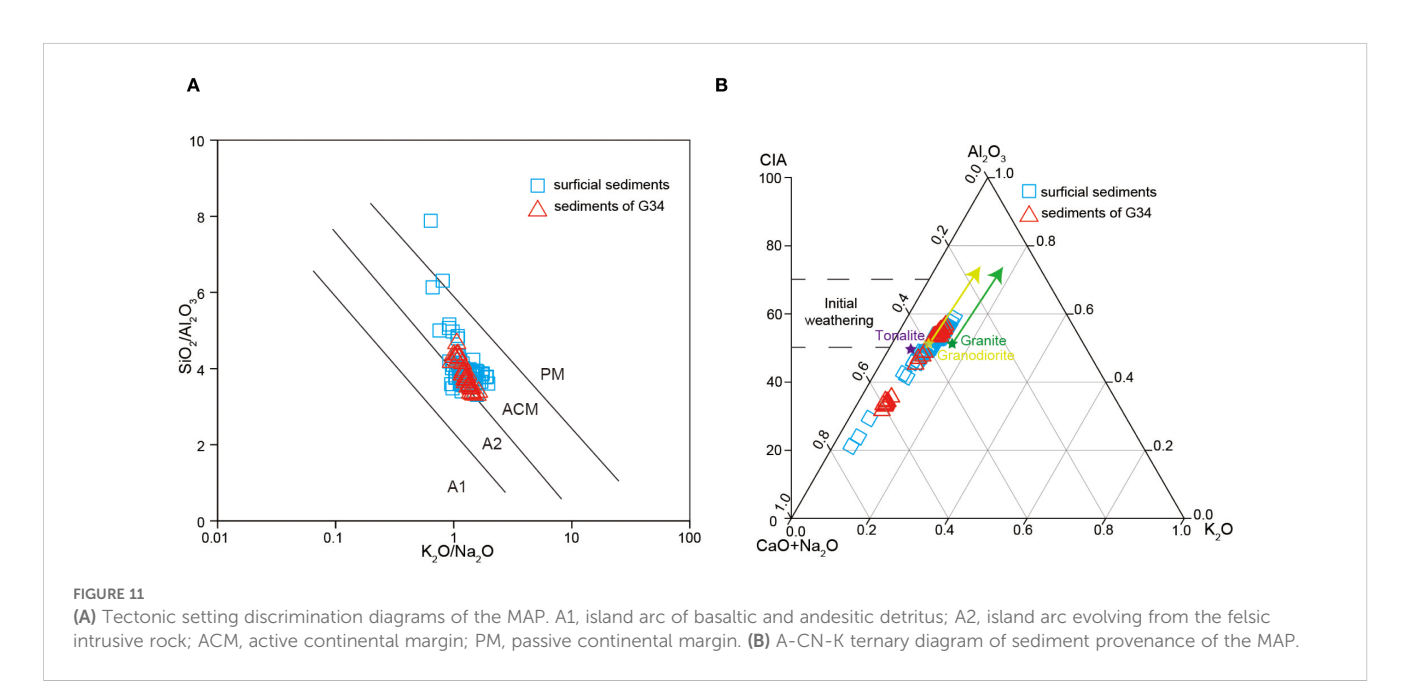
$$SO_4^{2-} + 2CH_2O \rightarrow H_2S + 2HCO_3^-$$
 (OSR) (2)

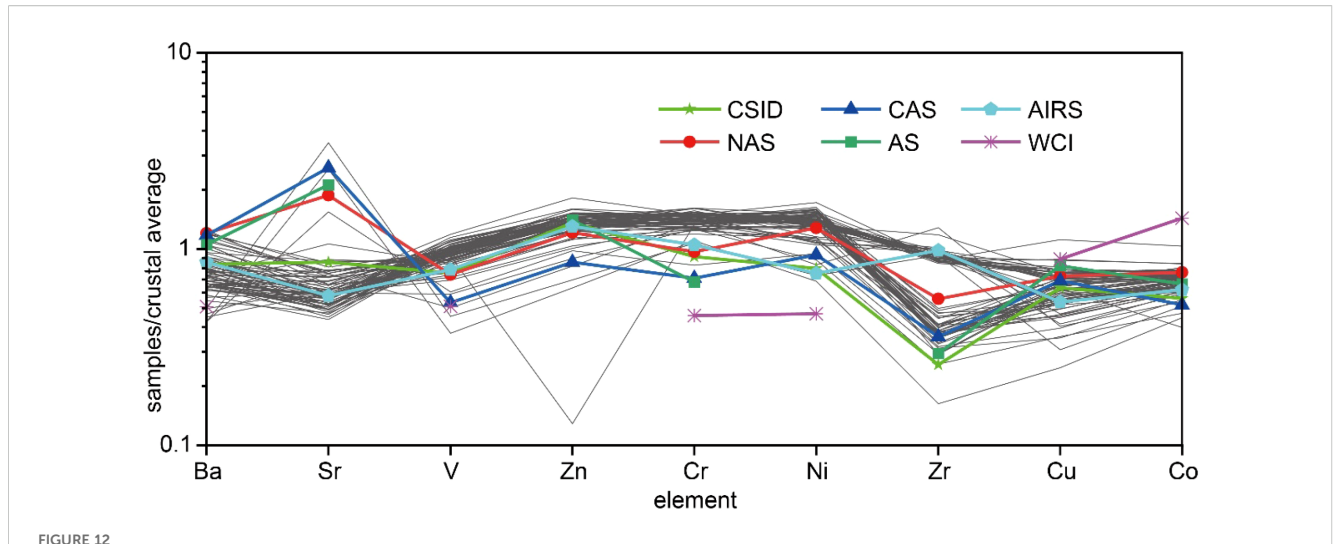
$$SO_4^{2-} + CH_4 \rightarrow HS^- + HCO_3^- + H_2O(AOM)$$
 (3)

Which requires sufficient methane to react with sulfate in a reductive manner, therefore the presence of sulfide zones in the surface sediments and the anomalous concentrations of U and Mo may be due to the high methane fluxes in this area. In areas of no methane seepage, sulfate is not consumed, resulting in a deep sulfate-methane interface (SMI), whereas, in areas of large scale methane seepage, CH4 fluids may surge upwards into the seawater-sediment interface and massively consume sulfate in the surface sediment pore water, resulting in a shallow SMI in this area. interface. The shallow burial of the SMI interface in the study area results in narrow oxidation and sub-oxidation zones in the sediments and the potential for H₂S from methane-sulfate reactions to transport upwards with the pore water into the surface sediments, resulting in sulfide zones enriched in Mo and U elements (Deng et al., 2017; Li et al., 2021; Gong et al., 2021).

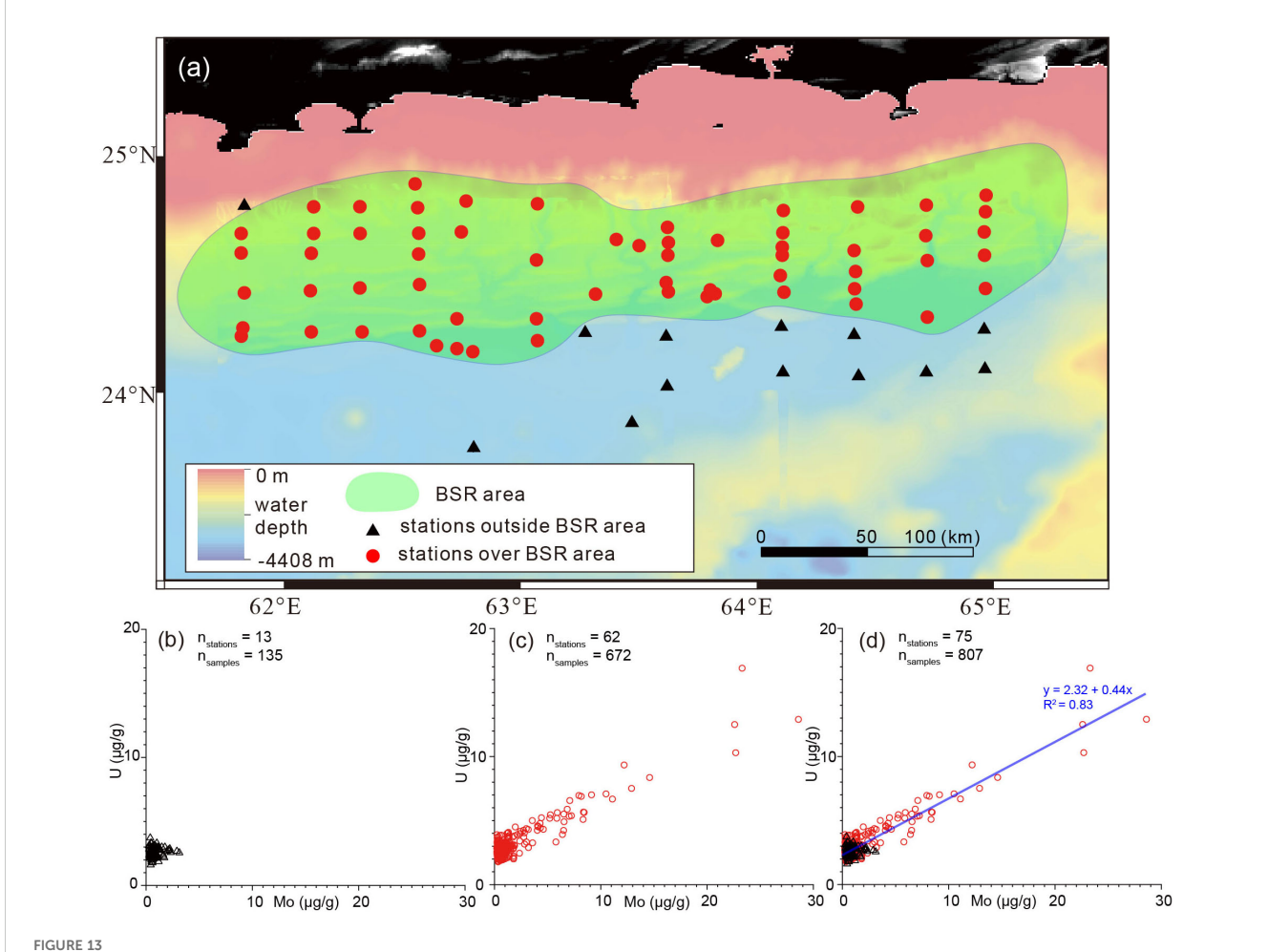
5 Conclusions

Based on analyses of grain size, geochemical properties, and clay minerals of surficial and core sediments collected from the MAP, the linkage between NGH distribution and sedimentary properties were discussed. The main results are as follows. (1) Surficial sediments were mainly controlled by hydrodynamic conditions of the Indus River. Along the Indus River channel, it is mainly infilled





Standardized curves of trace elements in the MAP. Crustal average (Taylor, 1964); CSID, surface sediments from the continental shelf off the Indus Delta (Khan et al., 2020); NAS & CAS, North Arabian Sea & Central Arabian Sea (Schnetger et al., 2000); AS, Arabian Sea (Sirocko et al., 2000); AIRS, Average Indus River Sediments (Clift et al., 2010); WCI, west coast India (Alagarsamy and Zhang, 2010).



Relationship between distribution of BSR and trace elements U and Mo in the Makran accretionary prism. (a)locations of sample stations and BSR area; (B) sample stations outside the BSR area; (C) sample stations over the BSR area; and (D) all samples. The BSR area of the study area was modified from (Smith et al., 2014).

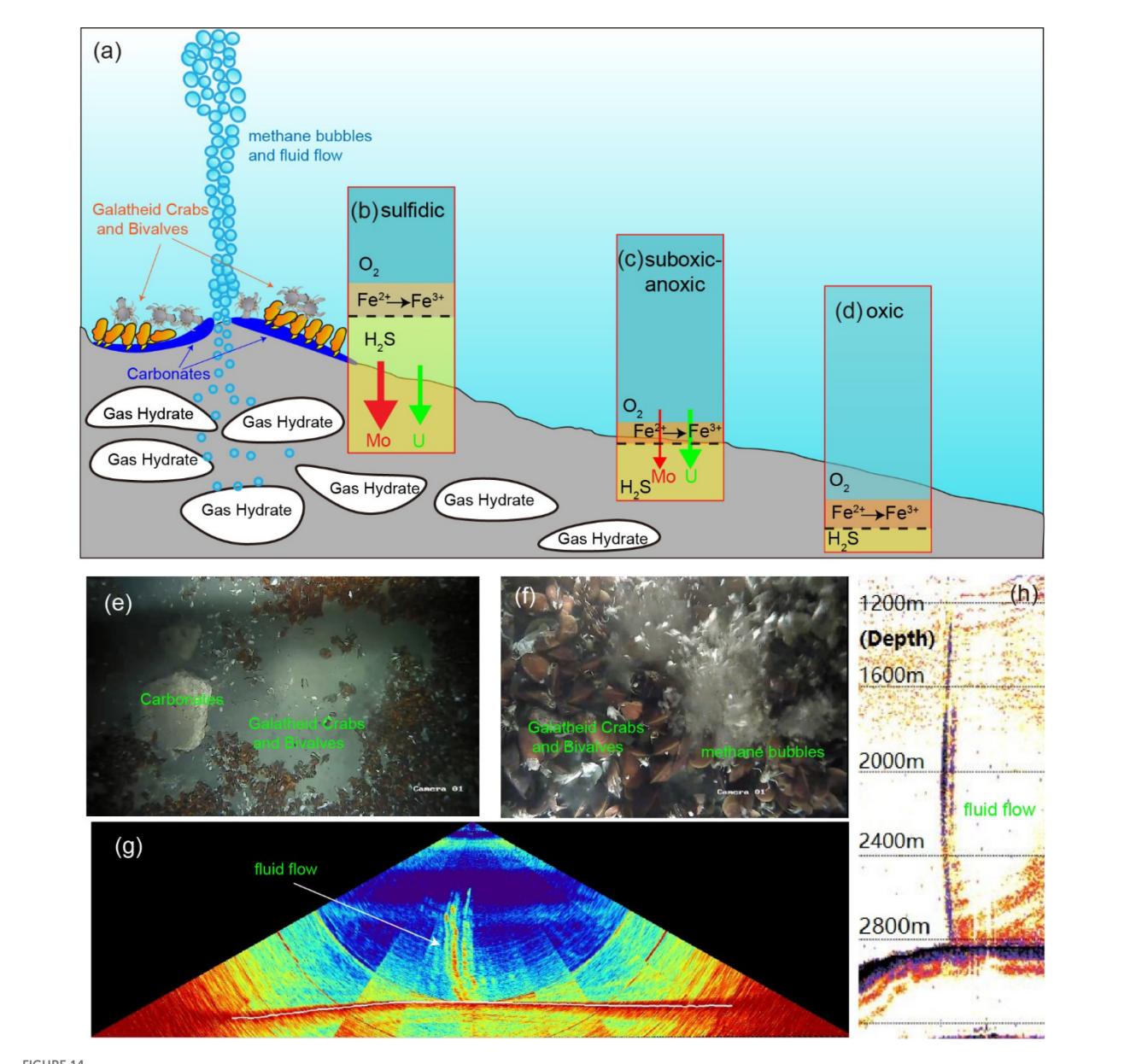


FIGURE 14
(A) Schematic diagram of the gas hydrate cold seep system (modified from Bohrmann and Torres, 2006; Delong, 2000); (B–D) relationships of Mo and U authigenic enrichment to benthic redox variation(modified from Algeo and Tribovillard, 2009); (E, F) biota and carbonates in the MAP cold seep area revealed by underwater imaging; (G, H) detection of cold seep fluid flow using multibeam and sub-bottom profiling aboard the R/V "Hai Yang Di Zhi Shi Hao".

with silt, while clays are mainly distributed in the accretionary prism. The turbidity records gradually decrease from east to west, along the Indus River channel. (2) Illite and chlorite are the dominate clay minerals, indicating that the surficial sediments were mainly from weathering processes in the Tibet Plateau by the Indus River transport. The very-low contents of kaolinite and smectite indicate the lack of sediments from the Deccan Traps and the *in situ* hydrothermal materials. (3) Elements analysis indicates that elements Al, Mg, K, Fe, and Ti were terrigenous, mainly

distributed in the northern Makran accretionary prism, while elements Ca and P were from biogenic sources, mainly distributed in the southern part of the study area. (4) Based on these results, a close relationship between NGH distribution and sedimentary properties was observed, and we therefore proposed that the covariation between NGH distribution, BSR identification, and trace elements Mo and U holds the potentials in NGH investigation. The anomalies of U and Mo in surface sediments can be used to efficiently conduct reconnaissance for NGH.

Data availability statement

The raw data supporting the conclusions of this article will be made available by the authors, without undue reservation.

Author contributions

HW: Data curation, Formal Analysis, Methodology, Visualization, Writing – original draft. LY: Data curation, Formal Analysis, Investigation, Methodology, Visualization, Writing – review & editing. FW: Data curation, Writing – original draft. YL: Formal Analysis, Writing – original draft. YC: Writing – review & editing. ZZ: Data curation, Writing – original draft. MY: Investigation, Writing – original draft. YY: Data curation, Writing – original draft. HY: Writing – review & editing. XD: Investigation, Writing – review & editing. GH: Funding acquisition, Writing – review & editing.

Funding

The author(s) declare financial support was received for the research and/or publication of this article. This research was funded by the National Natural Science Foundation of China (42476234, and U2244222), National Key R&D Program of China (2023YFC2809100), and the Geological Survey Projects of China Geology Survey (DD20230068).

Acknowledgments

We are grateful to all the crew and scientists from China and Pakistan for their work on the China-Pakistan Joint Marine Scientific Expedition during 2018-2019. We thank Jinlian Wang for grain-size analysis, Peixin Lai for analyzing clay minerals, and Qiang Li and Tianbang Yang for their helps in geochemical measurements. All data that support the findings of this study are available from the corresponding authors upon request hqyao@163.com.

Conflict of interest

The authors declare that the research was conducted in the absence of any commercial or financial relationships that could be construed as a potential conflict of interest.

Generative Al statement

The author(s) declare that no Generative AI was used in the creation of this manuscript.

Any alternative text (alt text) provided alongside figures in this article has been generated by Frontiers with the support of artificial intelligence and reasonable efforts have been made to ensure accuracy, including review by the authors wherever possible. If you identify any issues, please contact us.

Publisher's note

All claims expressed in this article are solely those of the authors and do not necessarily represent those of their affiliated organizations, or those of the publisher, the editors and the reviewers. Any product that may be evaluated in this article, or claim that may be made by its manufacturer, is not guaranteed or endorsed by the publisher.

References

Alagarsamy, R., and Zhang, J. (2010). Geochemical characterization of major and trace elements in the coastal sediments of India. *Environ. Monit Assess.* 161, 161–176. doi: 10.1007/s10661-008-0735-2

Algeo, T. J., and Rowe, H. (2012). Paleoceanographic applications of trace-metal concentration data. *Chem. Geology* 324–325, 6–18. doi: 10.1016/j.chemgeo.2011.09.002

Algeo, T. J., and Tribovillard, N. (2009). Environmental analysis of paleoceanographic systems based on molybdenum-uranium covariation. *Chem. Geology* 268, 211–225. doi: 10.1016/j.chemgeo.2009.09.001

Alizai, A., Hillier, S., Clift, P. D., Giosan, L., Hurst, A., Van der Pluijm, B., et al. (2012). Clay mineral variation in the Indus Delta and on the western continental shelf of India: implications for sediment transport and weathering. *Geochem. Geophys. Geosystems.* 13, Q01001. doi: 10.1029/2011GC003773

Avinash, K., Kurian, P. J., Warrier, A. K., Shankar, R., Vineesh, T. C., and Ravindra, R. (2016). Sedimentary sources and processes in the eastern Arabian Sea: Insights from environmental magnetism, geochemistry and clay mineralogy. *Geosci. Front.* 7, 253–264. doi: 10.1016/j.gsf.2015.05.001

Biscaye, P. E. (1965). Mineralogy and sedimentation of recent deep-sea clay in the Atlantic Ocean and adjacent seas and oceans. *Geological Soc. America Bull.* 76, 803–832. doi: 10.1130/0016-7606(1965)76[803:MASORD]2.0.CO;2

Bohrmann, G., Bahr, A., Brinkmann, F., Kassner, N., Kutterolf, S., Schleicher, A., et al. (2008). Cold seeps of the Makran subduction zone (Continent margin of Pakistan): R/V

Meteor cruise report M74/3: M74, Leg 3, Fujairah-Male, 30 Oct.- 28 Nov. 2007. Berichte, Fachbereich Geowissenschaften, Universitat Bremen, Bremen, Germany, 1–161.

Bohrmann, G., and Torres, M. E. (2006). "Gas hydrates in marine sediments," in Marine Geochemistry. Eds. H. D. Schulz and M. Zabel (Springer, Berlin, Heidelberg). doi: $10.1007/3-540-32144-6_14$

Bourget, J., Zaragosi, S., Ellouz-Zimmermann, N., Mouchot, N., Garlan, T., Schneider, J., et al. (2011). Turbidite system architecture and sedimentary processes along topographically complex slopes: the Makran convergent margin. *Sedimentology* 58, 376–406. doi: 10.1111/j.1365-3091.2010.01168.x

Burdanowitz, N., Gaye, B., Hilbig, L., Lahajnar, N., Luckge, A., Rixen, T., et al. (2019). Holocene monsoon and sea level-related changes of sedimentation in the northeast Arabian Sea. *Deep-Sea Res. Part II* 166, 6–18. doi: 10.1016/j.dsr2.2019.03.003

Burgath, M. P., von Rad, U., Roeser, H. A., and Gaedicke, C.. (2002). Fluid-venting signatures in the Makran accretionary wedge, offshore Pakistan: results from multibeam bathymetry and seismic imaging. *Geo-Marine Letters* 22, 97–108. doi: 10.1007/s00367-002-0105-7

Calvert, S. E., and Pedersen, T. F. (1993). Geochemistry of recent oxic and anoxic marine sediments: Implications for the geological record. *Mar. Geology* 113, 67–88. doi: 10.1016/0025-3227(93)90150-T

Campbell, K. A. (2006). Hydrocarbon seep and hydrothermal vent palaeoenvironments and palaeontology: past developments and future research

directions. Palaeogeography Palaeoclimatology Palaeoecol. 232, 362–407. doi: 10.1016/j.palaeo.2005.06.018

- Chen, H., Xu, Z., Cai, M., and Li, T. (2019). Provenance of clay-sized detrital sediments and its paleoenvironmental implications at Site U1456 in the eastern Arabian Sea since 30ka. *Earth Sci.* 44, 2803–2817. doi: 10.3799/dqkx.2018.185
- Clemens, S. C., and Prell, W. L. (2003). A 350,000 year summer monsoon multi-proxy stack from the Owen Ridge, Northern Arabian Sea. *Mar. Geology* 201, 35–51. doi: 10.1016/S0025-3227(03)00207-X
- Clift, P. D., Giosan, L., Carter, A., Garzanti, E., Eynatten, H. V., Webb, A. A. G., et al. (2010). "Monsoon control over erosion patterns in the Western Himalaya: possible feedbacks in the tectonic evolution," in *Monsoon evolution and tectonics-climate linkage in Asia*, vol. 342. Eds. P. D. Clift, R. Tada and H. Zheng (London, UK: Geol Soc Spec Publ), 185–218.
- Delong, E. F. (2000). Microbiology: resolving a methane mystery. Nature 407, 577–579. doi: 10.1038/35036677
- Deng, Y., Fang, Y., Zhang, X., Chen, F., Wang, H., Ren, J., et al. (2017). Trace element geochemistry of sediments in Qiongdongnan Area, the South China Sea, and its implications for gas hydrate. *Mar. Geology Quaternary Geology* 37, 70–81. doi: 10.16562/j.cnki.0256-1492.2017.05.007
- Dubinin, A. V. (2004). Geochemistry of rare earth elements in the ocean. *Lithology Mineral Resour.* 4, 289–307. doi: 10.1023/B:LIMI.0000033816.14825.a2
- Fleitmann, D., Burns, S. J., Mangini, A., Mudelsee, M., Kramers, J., Villa, I., et al. (2007). Holocene ITCZ and Indian monsoon dynamics recorded in stalagmites from Oman and Yemen (Socotra). *Quaternary Sci. Rev.* 26, 170–188. doi: 10.1016/j.quascirev.2006.04.012
- Gaedicke, C., Schlüter, H. U., Roeser, H. A., Rauch, T., Reichert, C., Meyer, H., et al. (2002). Origin of the northern Indus Fan and Murray Ridge, northern Arabian Sea: interpretation from seismic and magnetic imaging. *Tectonophysics* 355, 127–143. doi: 10.1016/S0040-1951(02)00137-3
- Ghose, I., Searle, M. P., Hacker, B. R., Kelemen, P. B., and Mehmood, N.. (2014). Jurassic to Neogene magmatism in the Muslim Bagh and Waziristan ophiolites, Pakistan: implications for the tectonic evolution of the western Indian Plate margin. *Tectonophysics* 636, 136–152. doi: 10.1016/j.tecto.2014.08.011
- Gong, J., Liao, J., Sun, J., Yang, C., Wang, J., He, Y., et al. (2016). Factors controlling gas hydrate accumulation in Makran accretionary wedge off Pakistan. *Mar. Geology Front.* 32, 10–15. doi: 10.16028/j.1009-2722.2016.12002
- Gong, J., Liao, J., Yin, W., Zhang, L., He, Y., Sun, Z., et al. (2021). Geochemical and mineral properties of Quaternary deep-sea sediments in the central-tropical Pacific and its response to the Mid-Pleistocene transition. *J. Mar. Sci. Eng.* 9, 1254. doi: 10.3390/jmse9111254
- Gong, J., Liao, J., Yin, W., Zhang, L., He, Y., Sun, Z., et al. (2018). Gas hydrate accumulation models of Makran accretionary wedge, northern Indian Ocean. *Mar. Geology Quaternary Geology* 38, 148–155. doi: 10.16562/j.cnki.0256-1492.2018.02.015
- Govil, P., and Naidu, P. D. (2008). Late Quaternary changes in depositional processes along the western margin of the Indus Fan. *Geo-Marine Lett.* 28, 1–6. doi: 10.1007/s00367-007-0083-1
- Grando, G., and McClay, K. (2007). Morphotectonics domains and structural styles in the Makran accretionary prism, offshore Iran. *Sedimentary Geology* 196, 157–179. doi: 10.1016/j.sedgeo.2006.05.030
- Guo, Q., Shields, G. A., Liu, C., Strauss, H., Zhu, M., Pi, D., et al. (2007). Trace element chemostratigraphy of two Ediacaran-Cambrian successions in South China: implications for orangosedimentary metal enrichment and silicification in the Early Cambrian. *Palaeogeography Palaeoclimatology Palaeoecol*. 254, 194–216. doi: 10.1016/j.palaeo.2007.03.016
- Holbrook, W. S., Hoskins, H., Wood, W. T., Stephen, R. A., Lizarralde, D, Leg 164 Science Party, et al. (1996). Methane hydrate and free gas on the Black Ridge from vertical seismic profiling. *Science* 273, 1840–1843. doi: 10.1126/science.273.5283.1840
- Hutchison, I., Louden, K. E., White, R. S., Horsfield, S. J, Leg 23 Shipboard Scientific Party, et al. (1981). Heat-flow and age of the gulf of Oman. *Earth Planetary Sci. Lett.* 56, 252–262. doi: 10.1016/0012-821X(81)90132-1
- Jacob, K. H., and Quittmeyer, R. C. (1979). "The Makran region of Pakistan and Iran: trench-arc system with active plate subduction." in *Geodynamics of Pakistan*. (Geological Survey of Pakistan), 305–317.
- Kessarkar, P. M., Rao, V. P., Ahmad, S. M., and Anil Kumar, A.. (2003). Clay minerals and Sr–Nd isotopes of the sediments along the western margin of India and the Indus Delta: implications to sediment sources. *Geophys. Res. Lett.* 30, 1184. doi: 10.1029/2002GL016031
- Khan, A. A., Haredy, R., and Inam, A. (2020). Geochemistry and sedimentary sources of the surface sediments from the continental shelf off the indus delta, Pakistan. *Thalassas* 36, 61–74. doi: 10.1007/s41208-019-00168-w
- Khan, M., and Liu, Y. K. (2019). Geodynamic evolution of the offshore Indus Basin Pakistan: the western Indian Plate passive continental margin. *Geophys. J. Int.* 217, 1366–1386. doi: 10.1093/gji/ggz091
- Kolla, V., Henderson, L., and Biscaye, P. E. (1981). Clay mineralogy and sedimentation in the western Indian Ocean. *Deep Sea Research Part A* 28, 613–625. doi: 10.1016/0198-0149(81)90042-8
- Kopp, C., Fruehn, J., and Flueh, E. R. (2000). Structure of the Makran subduction zone from wide-angle and reflection seismic data. *Tectonophysics* 329, 171–191. doi: 10.1016/S0040-1951(00)00195-5

- Kukowski, N., Schillhorn, T., and Huhn, K. (2001). Morphotectonics and mechanics of the central Makran accretionary wedge off Pakistan. *Mar. Geology* 173, 1–19. doi: 10.1016/S0025-3227(00)00167-5
- Li, Q., Yang, T., Zhuang, C., Deng, X., Wang, H., and Yu, M. (2021). Geochemical characteristics of the sediments at site G16 of the Makran accretionary wedge, the northern Arabian Sea, and their implications for gas hydrates. *Mar. Geology Quaternary Geology* 41, 161–169. doi: 10.16562/j.cnki.0256-1492.2020091802
- Liu, Z., Wang, H., Hantoro, W. S., Sathiamuthy, E., Colin, C., Zhao, Y., et al. (2012). Climatic and tectonic controls on chemical weathering in tropical Southeast Asia (Malay Peninsula, Borneo and Sumatra). *Chem. Geology* 291, 1–12. doi: 10.1016/j.chemgeo.2011.11.015
- Luckge, A., Doose-Rolinski, H., Khan, A. A., Schulz, H., and von Rad, U. (2001). Monsoonal variability in the northeastern Arabian Sea during the past 5000-years: geochemical evidence from laminated sediments. *Palaeogeography Palaeoclimatology Palaeoecol.* 167, 273–286. doi: 10.1016/s0031-0182(00)00241-8
- März, C., Hoffmann, J., Bleil, U., De Lange, G. J., and Kastern, S. (2008). Diagenetic changes of magnetic and geochemical signals by anaerobic methane oxidation in sediments of the Zambezi deep-sea fan (SW Indian Ocean). *Mar. Geology* 255, 118–130. doi: 10.1016/j.margeo.2008.05.013
- Maynard, J. B., Valloni, R., and Yu, H. S. (1982). Composition of modern deep-sea sands from arc-related basins. *Geological Soc. London Special Publications* 10, 551–561. doi: 10.1144/GSL.SP.1982.010.01.36
- Milkov, A. V. (2000). Worldwide distribution of submarine mud volcanoes and associated gas hydrate. *Mar. Geology* 167, 29–42. doi: 10.1016/S0025-3227(00)00022-0
- Mouchot, N., Loncke, L., and Mahieux, G. (2010). Recent sedimentary processes along the Makran trench (Makran active margin, off Pakistan). *Mar. Geology* 271, 17–31. doi: 10.1016/j.margeo.2010.01.006
- Nesbitt, H. W., and Young, G. M. (1982). Early Proterozoic climates and plate motions inferred from major element chemistry of Lutites. *Nature* 299, 715–717. doi: 10.1038/299715a0
- Prins, M. A., Postma, G., Cleveringa, J., Cramp, A., and Kenyon, N. H. (1999). Controls on terrigenous sediment supply to the Arabian Sea during the late Quaternary: the Indus Fan. *Mar. Geol.* 158, 241–254. doi: 10.1016/S0025-3227(98)00159-8
- Rodriguez, M., Chamot-Rooke, N., Huchon, P., Fournier, M., and Delescluse, M. (2014). Tectonics of the dalrymple trough and uplift of the murray ridge (NWIndian ocean). *Tectonophysics* 646, 1–17. doi: 10.1016/j.tecto.2014.08.001
- Römer, M., Sahling, H., Pape, T., dos Santos Ferreira, C., Wenzhöfer, F., Bohrmann, G., et al. (2012). Quantification of gas bubble emissions from submarine hydrocarbon seeps at the Makran continent margin (offshore Pakistan). *J. Geophysical Res.* 117, 1–19. doi: 10.1029/2012IC008115
- Schnetger, B., Brumsack, H.-J., Schale, H., Hinrichs, J., and Dittert, L. (2000). Geochemical characteristics of deep-sea sediments from the Arabian Sea: a high-resolution study. *Deep-Sea Res.* 47, 2735–2768. doi: 10.1016/S0967-0645(00)00047-3
- Shanmugam, G. (1994). The Bouma sequence and the turbidite mind set. *Earth Sci. Rev.* 42, 201-229. doi: 10.1016/S0012-8252(97)81858-2
- Shanmugam, G. (2002). Ten turbidite myths. Earth Sci. Rev. 58, 311–341. doi: 10.1016/0007-6813(81)90122-1
- Shepard, F. P. (1954). Nomenclature based on sand-silt-clay ratios. J. Sedimentary Petrology 24, 151–158. doi: 10.1306/D4269774-2B26-11D7-8648000102C1865D
- Sirocko, F., Garbe-Schönberg, D., and Devey, C. (2000). Processes controlling trace element geochemistry of Arabian Sea sediments during the past 25,000 years. *Glob Planet Chang* 26, 217–303. doi: 10.1016/S0921-8181(00)00046-1
- Smith, G. L. (2013). The Makran accretionary prism: sediment thickness and structure at the deformation front. $Geological\ Society$, London, Special Publications 372, 281–294. doi: 10.1144/SP372.13
- Smith, G. L., McNeill, L. C., Henstock, T. J., Arraiz, D., and Spiess, V. (2014). Fluid generation and distribution in the highest sediment input accretionary margin, the Makran. *Earth Planetary Sci. Lett.* 403, 131–143. doi: 10.1016/j.epsl.2014.06.030
- Smith, G. L., McNeill, L. C., Henstock, T. J., Arraiz, D., and Spiess, V. (2012). The structure and fault activity of the Makran accretionary prism. *J. Geophysical Res.* 117, 1–17. doi: 10.1029/2012JB009312
- Su, M., Yang, R., Wu, N., Zhang, H., Zhang, X., Liang, J., et al. (2014). Structural characteristics in the Shenhu area, northern continent slope of South China Sea, and their influences on gas hydrate. *Acta Geological Sin.* 88, 318–326. doi: 10.1111/1755-6724.12261
- Taylor, S. R. (1964). Abundance of chemical elements in the continental crust: a new table. *Geochim Cosmochim Acta* 28, 273–1285S. doi: 10.1016/0016-7037(64)90129-2
- Thamban, M., Kawahata, H., and Purnachandra, V. (2007). Indian summer monsoon variability during the holocene as recorded in sediments of the Arabian sea: timing and implications. *J. Oceanography* 63, 1009–11020. doi: 10.1007/s10872-007-0084-8
- Thamban, M., Purnachandra, V., and Schneider, R. R. (2002). Reconstruction of late Quaternary monsoon oscillations based on clay mineral proxies using sediment cores from the western margin of India. *Mar. Geology* 186, 527–539. doi: 10.1016/S0025-3227 (02)00268-2
- Tribovillard, N., Algeo, T. J., Lyons, T., and Riboulleau, A. (2006). Trace metals as paleoredox and paleoproductivity proxies: an update. *Chem. Geology* 232, 12–32. doi: 10.1016/j.chemgeo.2006.02.012

von Rad, U., Berner, U., Delisle, G., Doose-Rolinski, H., Fechner, N., Linke, P., et al. (2000). Gas and fluid venting at the Makran accretionary wedge off Pakistan. *Geo-Marine Lett.* 20, 10–19. doi: 10.1007/s003670000033

von Rad, U., Schaaf, M., Michels, K. H., Schulz, H., Berger, W. H., and Sirocko, F. (1999). A 5000-yr record of climate change in varved sediments from the oxygen minimum zone off Pakistan, northeastern Arabian Sea. *Quaternary Res.* 51, 39–53. doi: 10.1006/qres.1998.2016

Wang, J., Qiu, W., and Zhao, H. (2010). Tectonic settings analysis of gas hydrate deposits development. *Geological Sci. Technol. Inf.* 29, 100–106.

Wei, J., Wu, T., Deng, X., Haider, S. W., Kahkashan, S., and Yang, S. (2021). Seafloor methane emission on the Makran continental margin. *Sci. Total Environ.* 801, 149772. doi: 10.1016/j.scitoteny.2021.149772

Whitmarsh, R. B. (1979). Owen Basin off the southeast margin of Arabia and the evolution of the Owen Fracture Zone. *Geophysical J. R. Astronomical Soc.* 58, 441–470. doi: 10.1111/j.1365-246X.1979.tb01034.x

Wu, L., Yang, S., Liang, J., Lu, J., and Wang, H. (2010). Geochemical characteristics of sediments at site HQ-48 PC in Qiongdongnan area, the north of the South China Sea, and their implication for gas hydrates. *Geoscience* 24, 534–544.

Xie, L., Wang, J., Wu, N., Yang, S., and Zhang, H. (2013). Characteristics of authigenic pyrites in shallow core sediments in the Shenhu area of the northern South China Sea: Implications for a possible mud volcano environment. *Sci. China Earth Sci.* 56, 541–548. doi: 10.1007/s11430-012-4511-3

Xu, X. T., and Shao, L. Y. (2018). Limiting factors in utilization of chemical index of alteration of mudstones to quantify the degree of weathering in provenance. *J. Palaeogeogr. (Chinese Edition)* 20, 515–522. doi: 10.7605/gdlxb.2018.03.038a

Ye, H., Chen, J., Yao, Y., Liu, C., Li, Y., Wang, S., et al. (2025). How injecting CO_2 enhances marine natural gas hydrate exploitation: Review and prospect. *Renewable Sustain. Engergy Rev.* 222, 116011. doi: 10.1016/j.rser.2025.116011

Young, G. M., and Nesbitt, H. W. (1999). Paleoclimatology and provenance of the glaciogenic Gowganda Formation (Paleoproterozoic), Ontario, Canada: evidence from sediment geochemistry. *Geol. Soc. Am. Bull.* 111, 1330–1343. doi: 10.1130/0016-7606 (1999)111<1330:PAPOTG>2.3.CO;2

Yu, Z., Colin, C., Wan, S., Saraswat, R., Song, L., Xu, Z., et al. (2019). Sea level-controlled sediment transport to the eastern Arabian Sea over the past 600 kyr: clay minerals and Sr-Nd isotopic evidence from IODP site U1457. *Quaternary Sci. Rev.* 205, 22–34. doi: 10.1016/j.quascirev.2018.12.006

Zahid, A., Barfod, G. N., Khan, A. A., Dahlquist, J. A., and Kiani, S. H. (2015). Geochronology and geochemistry of the northernmost exposures of the Deccan Traps, Pakistan: implications for the origin of the Reunion plume. *Lithos* 232, 320–330. doi: 10.1016/j.lithos.2015.06.022

Zhang, Z., Deng, X., Yao, H., Li, B., Wang, H., He, G., et al. (2021). A preliminary study on geomorphological characteristics and genetic mechanism of pockmarks in the Makran accretionary prism, northern Arabian Sea. *Geo-Marine Lett.* 41, 1–16. doi: 10.1007/s00367-021-00704-9

Zhang, M., Sun, X., Lu, Y., Wang, X., and Zhang, Y. (2011). Mineralogy of authigenic tube pyrite from the Southwest Taiwan Basin of South China Sea and its tracing significance for gas hydrate. *Mineral Deposits* 30, 725–734.

Zhang, G., Zhu, Y., and Xu, H. (2003). Gas hydrate on the passive continental margin and its pool formation process. *Geological Rev.* 49, 181–186. doi: 10.1007/BF02873153